Pattern identification in systems with S(1) symmetry

Rory Hartong-Redden and Rouslan Krechetnikov

Phys. Rev. E **84**, 056212 — Published 15 November 2011

DOI: 10.1103/PhysRevE.84.056212

On pattern identification in systems with $S(1)$ symmetry

Rory Hartong-Redden
Department of Physics & Astronomy, Northwestern University, Evanston, IL 60208

Rouslan Krechetnikov
Department of Mechanical Engineering, UCSB, Santa Barbara, CA 93106

This work is devoted to pattern identification in systems with $S(1)$ symmetry based on limited experimental data. As we demonstrate, such pattern identification is complicated by the lack of a theoretical basis as well as by the presence of experimental uncertainties, and possible overlapping and missing points in the data. The study is motivated by a recent finding of physical systems where instabilities of different wavenumbers may co-exist and thus lead to several single-wavenumber patterns superimposed with a random phase-shift between them. As shown in this work, such patterns cannot be identified with Fourier analysis as well as direct measurement of the wavenumbers is not possible. We present both a constructive theoretical approach, which establishes the conditions under which the structure of such patterns is identifiable, and an example of application – the crown structure analysis in the drop splash problem. For the latter study a new experimental setup is developed based on high-speed stereo photography, which produces data suitable for a quantitative analysis of the observed patterns.

Keywords: pattern identification, frustration, symmetry

I. INTRODUCTION

A. Motivation

There are many natural and engineering systems, which exhibit pattern formation and are defined on periodic spatial or time domains: among them are coupled oscillators [1], oscillatory convection in binary mixtures [2], numerous astrophysical phenomena [3–6], synchronous rhythmic flashing of fireflies [7], along-the-edge instabilities of accelerating liquid sheets [8], crown patterns in the drop splash phenomena [9], to mention a few. In this work we consider systems where patterns are formed due to instabilities with several wavenumbers excited at the same growth rate. One recent example refers to along-the-edge instability of liquid sheets [8, 10, 11], where it was found that the linear evolution of the interfacial perturbation f (or its Fourier coefficient f_{kn}, $k \in \mathbb{R}$ and $n \in \mathbb{Z}$), is governed by the dispersion relation:

$$\lambda^2 = -\kappa\left(\sigma^{-1}\kappa^2 + 1\right), \tag{1}$$

where λ is the growth rate, $\kappa = \pm\sqrt{n^2 + k^2}$ the two-dimensional wavenumber, and σ the bifurcation parameter. Since the growth rate λ depends only on the modulus of the two-dimensional wavenumber κ, the maximum growth rate $\lambda_{\max}$ is achieved at $\kappa_{\max} = \sqrt{\sigma/3}$ and thus if $\kappa_{\max} > n \geq 1$, there exists several critical wavenumbers $k_c^{(i)}$, parameterized by $i = 0, \ldots, n$, with the same growth rate $\lambda_{\max}$.

At the linear level, the above result implies that if only one critical wavenumber is excited, then the pattern is single-wavenumber, while for higher values of σ more than one critical wavenumber can be excited such that the picture becomes 'frustrated', cf. figure 1b, as was discovered recently in certain regimes of the drop splash phenomena [9]. The frustrated picture occurs due to randomness of the initial conditions, which are amplified and evolved into several superimposed single-wavenumber patterns of different wavenumbers and with random phase shifts between them.

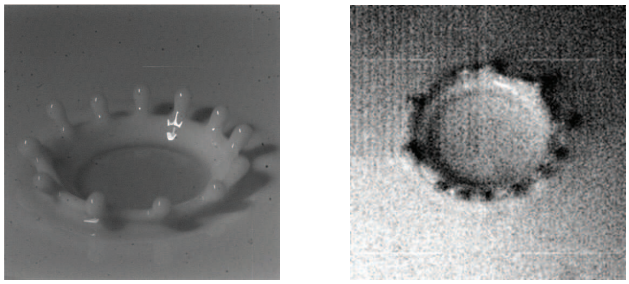

(a) (b)

FIG. 1: Patterns observed in the drop splash problem [9]: (a) single-wavenumber crown, (b) frustrated crown.

B. Key problem

Given the above theoretical example of frustrated pattern forming systems among many other natural phenomena, the natural question is how to identify such patterns based on experimental data. Namely, given experimental points, the collection of which is limited and could represent just peaks of the pattern (e.g. the location of spikes in figure 1), can one decompose the pattern into single-wavenumber subpatterns with random phase shifts between them? As discussed below, such patterns cannot be identified with Fourier analysis as well as direct measurement of the wavenumbers is not possible.

In this work we focus on one-dimensional systems with $S(1)$ symmetry, i.e. circle group, though the results are readily applicable to systems with isomorphic to $S(1)$ symmetry groups $SO(2)$, $\mathbb{T}$, and $\mathbb{R}/\mathbb{Z}$ as well as generalizable to higher dimensions. Therefore, our data are a list of points of the form $\Theta = \{\theta_1, \ldots, \theta_n\}$ and its underlying pattern structure is the subject of this study. For example, for the spatial domain case in

the context of the drop splash crown shown in figure 1, each θ_i represents the angle location of an individual crown spike on the interval $[0, 2\pi)$. In the time domain case, the data could be signals of several flashing fireflies [7] with rational ratios of periods [27] which naturally have a random phase shift between them: each θ_i would then be the time corresponding to a single flash. The problem on both time and spatial domains is to determine an underlying periodic structure of subpatterns of a given collection of data points Θ – the list of time events or spatial locations. Obviously, such sampling does not comply with the Nyquist-Shannon theorem [12] (i.e. if the period of our signal is $2\pi/n$ in the case of n spikes, the sampling rate should be n/π), which makes the discrete Fourier transform (DFT) approach impossible as will be shown below. However, here we have limited data, e.g. only the peaks of patterns, which, as we will show, are nevertheless sufficient to determine the pattern structure.

C. Paper outline

In what follows, in §II we first discuss the currently available tools and show their inapplicability to the resolution of the *key problem* formulated above. Next, we develop a theory (§III), which shows under which conditions patterns are identifiable in the ideal case (§III B), in the presence of scatter (§III C), as well as for the data with overlaps (§III D) and missing points (§III E). As an example of application of the developed theory, we use the data from the crown patterns in the drop splash problem (§IV), which required a new experimental technique (§IV A) to obtain data suitable for the analysis presented here. The examples of data analysis are given in §IV B. The discussion is concluded in §V with questions requiring further exploration.

II. INAPPLICABILITY OF KNOWN APPROACHES

In the case of a simple periodic signal one may use finite differences $\Delta\theta_{ij} = \theta_i - \theta_j$ to identify if such a pattern is periodic with a single period because the first off-diagonal elements of the matrix $\Delta\theta_{ij}$ give the period, e.g. for

$$\Theta = \{0, \pi/2, \pi, 3\pi/2\}, \tag{2}$$

this matrix becomes

$$\Delta\theta_{ij} = \begin{pmatrix} 0 & -\frac{\pi}{2} & -\pi & -\frac{3\pi}{2} \\ \frac{\pi}{2} & 0 & -\frac{\pi}{2} & -\pi \\ \pi & \frac{\pi}{2} & 0 & -\frac{\pi}{2} \\ \frac{3\pi}{2} & \pi & \frac{\pi}{2} & 0 \end{pmatrix}, \tag{3}$$

which tells us that the period is $\pi/2$. However once multiple periods are present, one must account for 'interference' and thus finite differences alone become insufficient and inefficient. In the case of substantial number of data points, a 'guess work' search for patterns is not feasible either because of the large number of possible combinations to analyze. Besides these direct inefficient approaches one may also think of application of the DFT, circular statistics, and the order parameter method to gain some insight into the pattern structure; however, as will be shown below, they do not allow one to resolve the key problem adequately and robustly.

A. Discrete Fourier transform

While the DFT is the standard tool for wavenumber or frequency analysis, it works well only for the data obeying the Nyquist-Sahnnon sampling theorem. For example, given the set (2) representing only the spike location, so that the corresponding points on the unit circle are

$$x_n = e^{i\,\theta_n},\ n = 0, \ldots, N-1, \tag{4}$$

the DFT

$$X_k = \sum_{n=0}^{N-1} x_n\, e^{-(2\pi i/N)\,k\,n},\ k = 0, \ldots, N-1, \tag{5}$$

gives $\boldsymbol{X} = \{0, 4, 0, 0\}$, i.e. the wavenumber $k = 1$ (corresponding to the wavelength 2π) is identified instead of the correct one $k = 4$. The same Fourier amplitudes $\boldsymbol{X}$ are obtained for the very different data set $\Theta = \{\pi/2, \pi/2, \pi/2, \pi/2\}$.

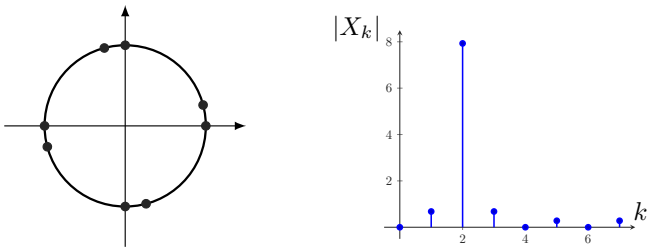

(a) (b)

FIG. 2: On inability of DFT to identify the structure of frustrated patterns: (a) two patterns of wavenumber 4 with the phase shift $\pi/12$, (b) power spectrum of DFT for the function in figure 2a; $X_2 = 7.93$.

Also, if we superimpose on the top of (2) the same wavenumber pattern (2) but with a phase shift $\phi = \pi/12$, then the DFT yields the distribution of the Fourier amplitudes as in figure 2b, which clearly illustrates that for a given set of data, the DFT does not help one to identify readily that there are two single-wavenumber patterns with $k = 4$ and the phase-shift $\phi = \pi/12$. Instead, one may may formally conclude that the pattern is of the wavenumber $k = 2$ with some noise. The useful insight one can get from the above examples is that the maximum of the power spectrum (in the ideal case without scatter) shown in figure 2b approximately equals to the number of pattern data points, e.g. in the considered example, it equals to $7.93 \simeq 8$, but there is a number of possible combinations of wavenumbers yielding the same maximum of the power spectrum. The number of possible subpattern combination grows with the number of data points and thus makes the DFT approach non-constructive. Therefore one needs a robust and systematic approach to decompose and identify patterns.

B. Circular statistics and order parameter

There are many systems, defined on a circle, which include problems with angles and time and require statistical analysis known as circular statistics [13]. One example from circular statistics is the measurement of the angles at which birds take flight [14]. The biologists are interested in how the data are clumped, i.e. if the birds leave in the same direction. Therefore, the circular statistics analysis is not intrinsically targeted to the identification and quantification of regular patterns, because a regular distribution of the birds departure angles would involve some sophisticated bird behavior!

More precisely, given a set of angles on the interval $[0, 2\pi)$, each of them defines a unit vector – adding up all these unit vectors results in a vector of length r, which can be rephrased more compactly using complex exponentials

$$r(m)\, e^{i\psi(m)} = \frac{1}{N}\sum_{j=1}^{N} e^{i\,\theta_j\, m},\ m \in \mathbb{N}, \tag{6}$$

where in the case $m = 1$ the expression $r\, e^{i\psi}$ is known as the *trigonometric moment* in circular statistics [13], and the *complex order parameter* in dynamical systems [1, 15]. Essentially, the complex order parameter can be interpreted as the collective rhythm produced by the collection of points on the unit circle in the complex plane. The complex order parameter is a useful diagnostic tool but its scope is to give a sense of how well ordered the system is: if $r(1) \simeq 0$, then the system is considered disordered as the unit vectors point in arbitrary uniformly distributed directions; if, on the other hand, $r(1) \simeq 1$, then the azimuths of a distribution are clumped in a particular direction. This is also known as the Rayleigh test. From the prospective of our analysis of patterns, when the order parameter is small, as in the case of regular pattern data with some scatter, then there is formally no difference between random and regular data from the point of view of circular statistics. The general case of (6), $m \geq 1$ introduced by Daido [16], allows one to characterize the synchronization properties and clustering: $r(m)\, e^{i\psi(m)}$ are the m-th Fourier modes of the distribution of phases. While the usual Kuramoto order parameter $r(1)\, e^{i\psi(1)}$ [15] is suitable for distributions with a single maximum, the higher order parameters are suitable for analyzing distributions with several maxima, often referred to as clusters. However, as we will show in §IV, even such a generalization is not suitable for identification of patterns composed of several single-wavenumber patterns with random phase shifts between them.

III. PATTERN IDENTIFICATION THEORY

A. Key notions

We begin by first introducing the key notions informally as motivated by the examples discussed in §§I and II. A *single-wavenumber pattern* is a set of elements which are regularly spaced on a circle and have at least two elements, e.g. (2). A *regular pattern* is a set consisting of a finite union [28] of single-wavenumber patterns with (potentially, random) phase shifts between them, cf. figure 2a. As a result, an *irregular pattern* does not have a regular structure and cannot be decomposed into a union of single-wavenumber patterns.

For systems with $S(1)$ symmetry it is natural to consider a data point as an angle $\theta \in [0, 2\pi)$, where the angles 0 and 2π are understood to represent the same point. A single-wavenumber pattern is described by a wavenumber $k \geq 2$ and a phase ϕ with respect to the origin $\theta = 0$, as illustrated in figure 3. Positive angles are measured in the counter-clockwise direction from the x-axis. The spacing between two consecutive elements of a single-wavenumber pattern is called the wavelength λ and related to the wavenumber by $k = 2\pi/\lambda$, which is an integer and also represents the number of points (spikes) on the unit circle.

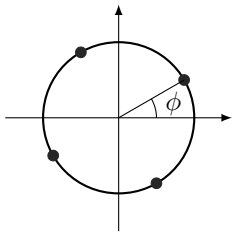

FIG. 3: An ideal single-wavenumber pattern, $\Theta(4, \phi)$, with wavenumber 4 and phase $\phi = \pi/6$ relative to a given, e.g. laboratory, system of coordinates.

If a single-wavenumber pattern with wavenumber k contains k elements it is said to be *complete*, i.e. not missing any elements. Expressing a regular pattern in terms of single-wavenumber patterns constitutes *pattern decomposition*.

B. Regular ideal patterns

We begin with the simplest case – the 'ideal pattern" – which is considered to be free from experimental scatter. The ideal pattern case will serve the basis for more general cases developed later in §§III C-III E.

1. *Definitions*

For the purpose of qualitative analysis, we will need a formal definition of ideal patterns.

Definition 1 (Ideal single-wavenumber pattern)**.** Let $\Theta = \{\theta_1, \ldots, \theta_k\}$ be a set of $\infty > k \geq 2$ elements. If Θ can be represented as

$$\{\theta_n \in [0, 2\pi)\,|\,\theta_n = n\,\lambda + \phi, \text{for } n = 0, \ldots, k-1\}, \tag{7}$$

where $\lambda = 2\pi/k$ is the wavelength and $\phi \in [0, \lambda)$ the phase shift, then $\Theta(k, \phi)$ is an *ideal single-wavenumber pattern*.

An ideal regular pattern is a set, which can be decomposed into a finite union of ideal single-wavenumber patterns, as formalized below.

Definition 2 (Ideal regular pattern)**.** Let $\mathbf{\Theta}$ be a finite set containing all elements of interest. If $\mathbf{\Theta} = \bigcup_{i=1}^{m} \Theta^{(i)}(k_i, \phi_i)$, where $\Theta^{(i)}$ is the i^{th} ideal single-wavenumber pattern such that $\Theta^{(i)} \bigcap \Theta^{(j)} = \emptyset$ if $i \neq j$, and m is the least number of ideal single-wavenumber patterns[29], then $\mathbf{\Theta}$ is an *ideal regular pattern*.

Note that permutations in this decomposition into single-wavenumber patterns do not lead to a new pattern. To clarify the terminology introduced above, consider the example in figure 3. Plotted are the angles from the set $\mathbf{\Theta} = \{\phi, \pi/2+\phi, \pi+\phi, 3\pi/2+\phi\}$ with $\phi = \pi/6$. By inspection we see that this set is a single-wavenumber pattern with the wavenumber $k = 4$ and the wavelength $\lambda = \pi/2$ because $\mathbf{\Theta} \equiv \Theta(4, \phi) = \{\theta_n \in [0, 2\pi) \,|\, \theta = \pi n/2 + \phi, \text{ for } n = 0, \ldots, 3\}$.

For the subsequent analysis, we will also need the difference matrix introduced in §II, which is a key step towards uncovering the regular decomposition of a set $\mathbf{\Theta} = \{\theta_1, \ldots, \theta_N\}$ with N elements. The difference $N \times N$ skew-symmetric matrix $\Delta\mathbf{\Theta}$ consists of differences between all pairs of elements in the set $\mathbf{\Theta}$:

$$\Delta\mathbf{\Theta}_{ij} = \theta_i - \theta_j. \tag{8}$$

Remark 1. The difference matrix $\Delta\mathbf{\Theta}$ contains $(N-1)N/2 = \frac{N!}{(N-2)!2!} = \binom{N}{2}$ possible unique entries; its lower triangular half of $\Delta\mathbf{\Theta}$ contains all the positive difference combinations, cf. (3).

2. *Pattern identification*

Now the idea is to demonstrate decomposability of ideal regular patterns.

Theorem 1. *If a given ideal regular pattern is complete and without overlapping elements, then there exists an algorithm which identifies it. The resulting pattern decomposition is unique.*

Proof. Let us demonstrate the existence of at least one algorithm capable of decomposing any given ideal regular pattern, which is complete and without overlaps, into ideal single-wavenumber patterns with some phase shifts between them. In order to initiate a decomposition of the given set $\mathbf{\Theta}$ of length N into ideal single-wavenumber patterns $\Theta^{(i)}(k_i, \phi_i)$, we first identify the wavelength λ of ideal single-wavenumber patterns. Let us consider differences between two elements of $\mathbf{\Theta}$

$$\Delta\mathbf{\Theta}_{ij} = \theta_i - \theta_j = (n_i\lambda + \phi_i) - (n'_j\lambda' + \phi_j), \tag{9}$$

for some $n_i, n'_j \in \mathbb{Z}^+$. Any pair of elements belong either to the same single-wavenumber pattern or to different single-wavenumber patterns. Should two elements *happen* to belong to the same single-wavenumber pattern, i.e. if $\theta_i, \theta_j \in \Theta^{(i)}$, then $\lambda = \lambda'$ and $\phi_i = \phi_j$, in which case equation (9) becomes

$$\Delta\mathbf{\Theta}_{ij} = (n_i - n'_j)\lambda, \; n_i - n'_j \in \mathbb{Z}^+, \tag{10}$$

which allows one to distinguish the elements θ_i of the set Θ obeying (10), which belong to that single-wavenumber pattern. Equation (10) states that the spacing between elements in an ideal single-wavenumber pattern are multiples of the wavelength λ of that pattern. In particular, for a single-wavenumber pattern of wavenumber $k = 2\pi/\lambda$ containing k elements, we should expect to find $\binom{k}{2} = \frac{k!}{2!(k-2)!}$ positive entries in the difference matrix $\Delta\mathbf{\Theta}$.

Given λ, equation (10) allows one to form a set of elements from $\Delta\mathbf{\Theta}_{ij}$, which belong to a single-wavenumber pattern with wavelength λ. This set of elements, which are spaced by multiples of λ, requires further consideration. Two complications may occur: (a) it may be that 'pathological' phase shifts between subpatterns of different wavenumbers coincide with the wavelength λ and thus give rise to spurious pairs of elements, or (b) there may be multiple single-wavenumber patterns with the same wavenumber and some phase shifts between them. Even though the situation (a) is highly improbable due to randomness of the initial conditions, those spurious elements are easy to exclude from the consideration since the wavenumber (and therefore the number of elements in the single-wavenumber pattern) is known. As for the situation (b), the individual same wavenumber patterns and the phase shifts between them can be identified based on the knowledge of the wavenumber. A search for possible single-wavenumber patterns is started with the largest wavenumber $k = N$, i.e. containing the total number of elements in $\mathbf{\Theta}$. Namely, starting with the largest wavenumber ensures that the fewest number of single-wavenumber patterns will be used in the decomposition. Once single-wavenumber patterns are identified, they are removed from the set $\mathbf{\Theta}$ and the process iterates until every element of $\mathbf{\Theta}$ belongs to a unique single-wavenumber pattern. By construction, the pattern decomposition is unique. □

3. *Subpatterns of single-wavenumber patterns*

In certain cases, a single-wavenumber pattern may be decomposed as a union of smaller *subpatterns*. A subpattern is simply another single-wavenumber pattern with a smaller wavenumber (larger wavelength), which is a subset of the larger single-wavenumber pattern under consideration. This idea of subpatterns will prove useful when analyzing patterns with overlaps in §III D.

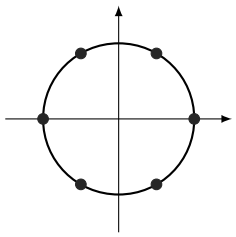

FIG. 4: An ideal single-wavenumber pattern $\Theta(6, 0)$.

We now clarify these ideas with an example. Referring to figure 4, where $\Theta(6,0) = \{\theta_n \in [0, 2\pi) | \, \theta = \pi n/3 \text{ for } n =$

$0, \ldots, 5\}$, we can observe that this single-wavenumber pattern with wavenumber 6 can be grouped into two sets of single-wavenumber patterns with wavenumber 3, or into three sets of single-wavenumber patterns with wavenumber 2:

$$\Theta(6,0) = \Theta^{(1)}(3,0) \bigcup \Theta^{(2)}(3,\pi/3)\,, \tag{11a}$$

$$= \Theta^{(3)}(2,0) \bigcup \Theta^{(4)}(2,\pi/3) \bigcup \Theta^{(5)}(2,2\pi/3)\,. \tag{11b}$$

In general, this leads to the following claim, the proof of which is straightforward.

Lemma 1. *Any ideal single-wavenumber pattern $\Theta(N,\phi)$, where N is not a prime number, may be expressed as a union of ideal single-wavenumber patterns of wavenumber p, where p is an integer divisor of N,*

$$\Theta(N,\phi) = \bigcup_{i=1}^{N/p} \Theta^{(i)}\left(p, \phi + \lambda_N (i-1)\right)\,. \tag{12}$$

C. Regular patterns with scatter

A natural generalization of ideal patterns is to consider the case of (non-ideal) regular patterns when the elements of $\boldsymbol{\Theta}$ have some uncertainty (experimental scatter) associated to them. As such, the following development is more relevant to actual measured data. It is natural to introduce non-ideal patterns by allowing deviations (residuals) from the ideal case. Hence, a regular pattern with scatter is defined about the corresponding ideal regular pattern by letting ϵ_i be the deviation of θ_i from the ideal case. A natural assumption is that the magnitude of the uncertainties $|\epsilon_i|$ is bounded from above by some constant δ. Such patterns are called *regular with scatter*, where the amount of scatter is quantified with the *scatter bound* δ.

Definition 3 (Single-wavenumber pattern with scatter)**.** Let $\Theta = \{\theta_1, \ldots, \theta_k\}$ be a set with k elements. If Θ admits the following representation $\{\theta_n \in [0, 2\pi) \,|\, \theta_n = n\lambda + \phi + \epsilon_n,\ \text{for } n = 0, \ldots, k-1,\ |\epsilon_n| \le \delta\}$, where $\lambda = 2\pi/k$ is the wavelength, $\phi \in [0, \lambda)$ the phase shift, and δ the scatter, then $\Theta(k, \phi, \delta)$ is a *single-wavenumber pattern with scatter*.

Figure 5 illustrates the correspondence between the two ways of viewing the same pattern. On the left is the unit circle with points θ_i shifted by ϵ_i from the ideal location. On the right is a plot in the (n, θ_n)-coordinates. All the points collapse to a line in the limit of vanishing scatter $\delta \to 0$. This graphical representation of a regular pattern naturally illustrates scatter and phase shifts, e.g. the phase shift is just the y-intercept of the line. One can apply standard error analysis [17] by considering $\Theta = \{\theta_1, \ldots, \theta_N\}$ as a series of measurements, which ideally should fall on a line $\theta_n = \lambda n + \phi$, where $\lambda = 2\pi/k$ and $k \in \mathbb{N}$ (cf. figure 5b).

As easy to see, the condition for a given pattern to be in the ideal regime is when two elements are not closer than twice the scatter δ, $\lambda > 2\delta$. Such spacing of the elements allows one

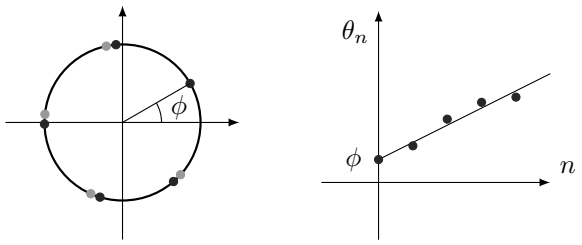

(a) (b)

FIG. 5: On the definition and identification of patterns with scatter: (a) a pattern with scatter (dark circles) defined relative to the ideal pattern (light circles), (b) representing a circular pattern on a graph: the points are plotted as coordinates (n, θ_n), where the line represents the ideal linear relationship $n\lambda + \phi$ with λ being the wavelength λ, ϵ_n is the residual between the line and the plotted point, $\epsilon_n = \theta_n - (n\lambda + \phi)$.

to avoid the ambiguity when two points lie within the scatter radius and effectively overlap. From a theoretical perspective, the two conditions – spacing of the elements and the pattern completeness – are sufficient to avoid the cases when patterns are not identifiable.

Theorem 2. *If a given regular pattern $\boldsymbol{\Theta}$ with scatter δ is complete and in the ideal regime, such that none of the two elements of $\boldsymbol{\Theta}$ are closer than twice the scatter, $\lambda > 2\delta$, then there exists an algorithm which identifies the pattern. The resulting pattern decomposition is unique.*

Proof. We will again demonstrate the existence of an algorithm which identifies regular patterns with scatter by providing the decomposition into single-wavenumber patterns with scatter. Let $\boldsymbol{\Theta}$ be a regular pattern with N elements which can be partitioned into single-wavenumber patterns with scatter δ. In the ideal regime, the single-wavenumber patterns are separated such that $\Theta^{(i)} \bigcap \Theta^{(j)} = \emptyset$ if $i \neq j$. Similar to the case without scatter, we begin by considering a difference between two elements of $\boldsymbol{\Theta}$

$$\Delta\boldsymbol{\Theta}_{ij} = \theta_i - \theta_j = (n_i\lambda + \phi_n + \epsilon_n) - (n'_j\lambda' + \phi_{n'} + \epsilon_{n'}), \tag{13}$$

for some indices $n_i, n'_j \in \mathbb{Z}^+$. In analogy to the ideal case considered in §III B, equation (13) may be simplified if θ_i and θ_j belong to the same single-wavenumber pattern with scatter. That is, $\theta_i, \theta_j \in \Theta^{(k)}$

$$\Delta\boldsymbol{\Theta}_{ij} = (n - n')\lambda + \epsilon_n - \epsilon_{n'}\,. \tag{14}$$

By the theorem assumption, $\epsilon_n, \epsilon_{n'}$ are both bounded by constant δ, so that the relation (14) gives

$$|\Delta\boldsymbol{\Theta}_{ij} - (n - n')\lambda| \le 2\delta. \tag{15}$$

Equation (15) is an exact analogy to equation (10) in the ideal case with the only difference that the scatter parameter δ introduces an inequality (the ideal equality case (10) is recovered in the limit $\delta \to 0$). Thus, the algorithm follows that of theorem 1 and therefore provides a unique pattern decomposition (provided $\lambda > 2\delta$). □

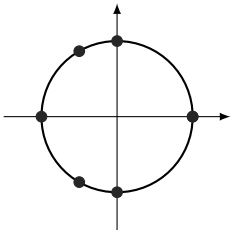

FIG. 6: Two overlapping single-wavenumber patterns with wavenumbers 3 and 4 which share the element $\theta = 0$.

Therefore, in the regular pattern regime with scatter, the analysis is straightforward and no 'pathological' cases need be considered because the points are spaced according to the conditions in theorem 2. With the modification of the equality (10) to the inequality (15), the algorithm is identical to the one presented for ideal regular patterns in §III B.

D. Regular patterns with overlaps

Until now, we have considered only regular patterns when no overlapping single-wavenumber patterns may occur. Figure 6 illustrates an ideal regular pattern with overlaps consisting of two single-wavenumber patterns, $\Theta(3, 0)$ and $\Theta(4, 0)$, which share one element, $\theta = 0$. A physical example and reasons for the presence of overlaps will be given in §IV E. Due to the fact that overlapping elements are 'double-counted', a regular pattern with overlaps has fewer elements than the sum of the elements of the constituent single-wavenumber patterns.

The presence of overlaps in a regular pattern requires the understanding of the origin of single-wavenumber patterns developed in §III B, as will become clear from the subsequent discussion.

Motivated by the example in figure 6 let us consider ideal regular patterns, which may contain overlapping ideal single-wavenumber patterns, while each component single-wavenumber pattern is complete.

Theorem 3. *If a given ideal regular pattern, possibly containing overlaps, consists of complete single-wavenumber patterns, then there exists an algorithm which identifies it. The resulting pattern decomposition is unique.*

Proof. Let us again demonstrate the existence of an algorithm which identifies ideal regular patterns potentially containing ideal single-wavenumber patterns with overlaps. Accommodating the presence of overlaps requires only a few modifications of the original algorithm developed in §III B. The main modification is to note that a given element $\theta_i \in \mathbf{\Theta}$ may belong to multiple single-wavenumber patterns. Therefore, subtracting single-wavenumber patterns as they are identified may affect other equally valid single-wavenumber patterns. One mechanism to avoid this complication is to test for and identify all possible single-wavenumber patterns with wavenumbers ranging from N to 2 without removing single-wavenumber patterns once they are identified. From lemma 1 on subpatterns, finding redundant subpatterns of a single-wavenumber pattern is trivial and guarantees a unique pattern decomposition. Once subpatterns are removed, all that remains are the largest possible single-wavenumber patterns, which constitute the decomposition of the ideal regular pattern. The rest of the algorithm is the same as in theorem 1. □

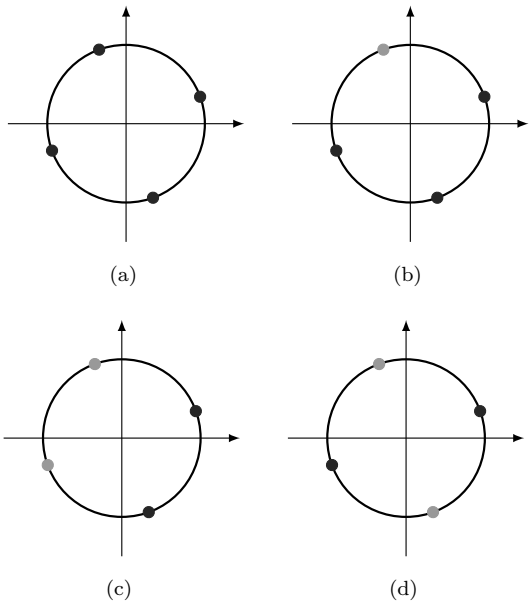

FIG. 7: On the definition of incomplete patterns (light circles are the removed elements): (a) the complete single-wavenumber pattern with wavenumber $k = 4$, (b) one element removed: the incomplete single-wavenumber pattern is identifiable, (c) two elements removed: the incomplete pattern is still identifiable, (d) two elements removed: the resulting single-wavenumber pattern ($k = 2$) cannot be identified as incomplete.

E. Incomplete patterns

Finally, we provide some considerations for the case of incomplete regular patterns, i.e. when there are missing points, which can be due to, for example, the limited ability to collect experimental data. These considerations lead to a proper definition of incomplete patterns and the conditions when they are identifiable. It is not straightforward, however, to define an incomplete pattern, because any given regular pattern can be considered to be the result of a larger pattern missing the appropriate elements. We illustrate this and other complexities with the following simple example of a regular single-wavenumber pattern $\Theta(4, \phi)$ in figure 7a. Let us remove some elements and consider whether the resulting incomplete pattern is identifiable. To identify an incomplete pattern, a minimal number of elements are added such that a regular pattern is completed.

In the first case, when only one element is removed, as shown in figure 7b, the incomplete pattern is identifiable and can be completed, because the grayed element can be added by extrapolating the obvious wavelength $\pi/2$ to the area of

missing spikes.

The second case deals with two elements, which can be removed in two ways. Figure 7c shows the result if two consecutive elements are removed. In this case, the incomplete pattern may be identified in the manner analogous to the one in figure 7b, since the wavelength is identifiable: the two grayed elements may be added back to make a single-wavenumber pattern with wavenumber 4. The other case, in which two non-adjacent elements are removed as in figure 7d, the 'incomplete' pattern is just a single-wavenumber pattern with wavenumber 2! Therefore, the incomplete pattern is not identifiable. The key distinction in this case from the former ones is that the removed elements constitute a subpattern, which is a single-wavenumber pattern on its own.

Therefore, a useful definition of an *incomplete pattern* is the one in which a pattern is identifiable.

Definition 4. An *incomplete regular pattern* Θ^I is a regular pattern, Θ^R, minus a subset of points $\Theta^- \subset \Theta^R$:

$$\Theta^I(k,\phi) = \Theta^R(k,\phi) \setminus \Theta^-, \tag{16}$$

where Θ^I is not a regular pattern in the sense of definition 2.

While the theory of incomplete pattern identification yet to be developed, probably in the context of a concrete application, one may conjecture that a sufficient condition for $\Theta^I(k,\phi)$ to be identifiable is if Θ^- is not regular, i.e. not decomposable into any single-wavenumber patterns.

IV. APPLICATION: CROWN PATTERNS IN THE DROP SPLASH PROBLEM

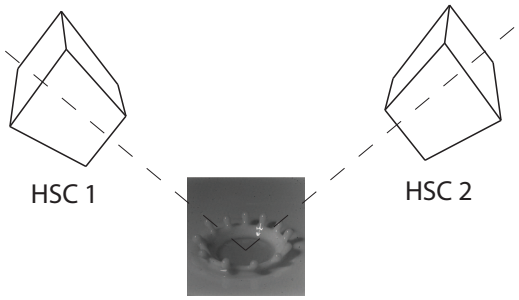

FIG. 8: Schematic of the experimental setup consisting of two synchronized high-speed cameras (HSC) oriented at different viewing angles.

The goal of this section is to provide an illustration of physical phenomena when the question of pattern identification arises and to demonstrate an experimental approach of obtaining the data suitable for the analysis offered in §III. The illustration comes from the drop splash problem [9]. Since the goal here is just to illustrate pattern identification theory, no attempt is made to perform a full study of the drop splash patterns, which is beyond the scope of the present paper.

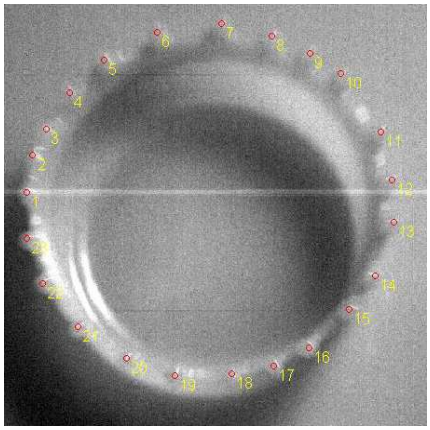

(a)

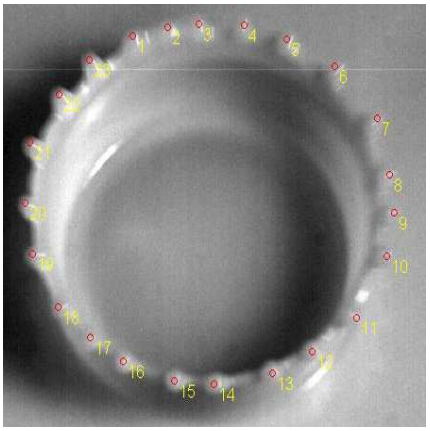

(b)

FIG. 9: (Color online) Stereo images of a drop splash crown with corresponding spikes (circles) labeled by number: (a) left image, (b) right image.

A. Experimental setup and data extraction

The key components of the experimental setup (cf. figure 8) necessary to collect the data suitable for the pattern identification analysis can be divided into two groups. The first group is responsible for measuring the physical parameters and generating the drop splash, which is discussed in detail in [9]. Namely, the droplet is created by pumping a liquid through a syringe at a consistent low flow rate ensuring that droplet formation is uniform. The syringe is positioned, with the help of a linear stepper motor, above a petri dish filled with a thin liquid film of controlled thickness.

The second group of components serves to capture the drop splash event. Since the drop splash event lasts over a fraction of a second, high-speed cameras (Phantom v5.1-5.2) are necessary to capture the dynamics, which is standard in the drop splash studies. However, since we are interested in the structure of the crown in space, we appeal to 3D high-speed photography, which is new in the context of the drop splash experiments; note that it is impossible to get accurate positions of the crown spikes using just one camera because (a) it

cannot be placed right above the drop splash and (b) the time-dependent dynamics of the crown is unknown. The setup in figure 8 cartoons how two high-speed cameras are positioned at two different viewing angles to generate a stereo video of the event. The cameras need to be calibrated and synchronized with a trigger to ensure that each of pair of frames correspond to the same time event.

1. *Stereo camera calibration and triangulation*

The basic idea of the stereo approach is that given two images of the same scene taken from different viewing positions, they are first matched and the difference between them allows one to recover the lost 3D dimension, i.e. the depth [18].

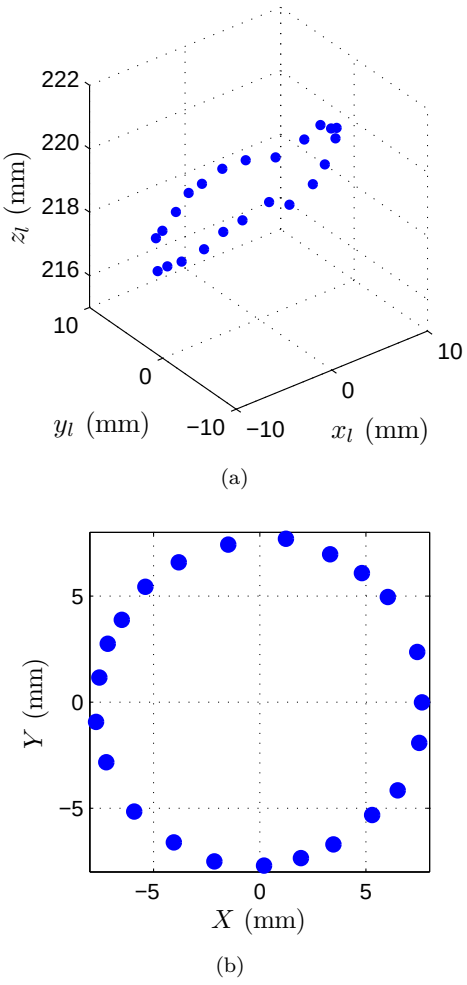

FIG. 10: Example of data reduction from the images in figure 9: (a) spike positions as a result of stereo triangulation in the reference frame of the left camera; circle size corresponds to the cumulative experimental uncertainty (§IV A 3), (b) data projected onto a plane and circle.

The practice of making physical measurements using images, known as photogrammetry, is over a century old; the historical development of camera models and calibration techniques may be found in [19]. The result of a 'camera calibration' is a model of the camera which translates between a point in an image and the light ray that is projected to that point, which is indispensable for relating the image features acquired with stereo photography to the laboratory coordinates. A stereo calibration consists of determining the position of the right camera reference frame with respect to the left camera (or vice versa). Beginning with the seminal work by Tsai [20], steady progress has been made towards the passive calibration of standard cameras [21, 22], which does not require any internal information about the camera, such as its focal length. Bouguet [23] has implemented the calibration procedure into a Matlab toolbox [24], which is used in our setup.

Stereo triangulation, i.e. the determination of a coordinate in 3D space from a pair of images, is possible once a stereo calibration has been performed. Stereo triangulation makes use of the fact that each pixel location on the image defines a ray as in human vision, hence determining a point in 3D space becomes a geometric problem of finding the point of intersection of two rays (or the closest point between the rays in the non-ideal case). Accuracies of various calibration routines, when an object of known geometry is compared to the geometry measured using a stereo triangulation method, have been reported to be one part in a thousand [20].

2. *Data extraction procedure*

We now give a detailed description of the data extraction procedure, which begins with a pair of images and ends with a set of angles $\mathbf{\Theta}$.

The first step is to identify the corresponding spikes in each of the left and right images. The corresponding spikes from the left and right images are shown in figure 9, where same numbers correspond to the same spike[30]. It should be noted that the ability to recognize the same object from different perspectives is known as the 'correspondence problem' of stereo vision [25], which is complicated by noise, obstructions, and reflective properties of the viewed objects; this remains to be a generally unsolved problem. Therefore, the process of actually determining which spikes correspond between the left and right images is done 'by hand'. For accurate correspondence, it is necessary to have a visible and identifiable point on the object in both camera views. For the purposes of the present experiment, such a point is the tip of a particular spike. We intentionally used slightly out of focus photos as it does not affect the accuracy of stereo triangulation.

The two pixel coordinate pairs, $(\widetilde{x}_l, \widetilde{y}_l)$ and $(\widetilde{x}_r, \widetilde{y}_r)$, of a given point from the left and right cameras, respectively, are the input for the stereo triangulation function. The latter gives the position (x_l, y_l, z_l) of the point in the reference frame of the left camera, cf. figure 10a; the details of stereo triangulation may be found in [23].

With the 3D data now available, the next step is to reduce the data to a set of angles on the unit circle. Since the point (x_l, y_l, z_l) is given in the frame of the left camera, which position relative to the location of the crown rim is arbitrary, an

ideal (flat) rim would be just a set of points lying on a circle which has been rotated and translated. Therefore, instead of directly fitting the spike coordinates to a general rotated and translated circle in 3D space, we break up the task into two linear steps: fitting to a plane, and then to a circle in that plane.

A plane is fitted to the data in the least-squares sense, which gives a plane defined by its normal $\boldsymbol{z}'$ vector. To rotate this plane to the laboratory frame of reference defined by normal $\boldsymbol{Z}$ to the horizontal plane, we make use of Rodrigues' rotation formula [26]. The direction of a desired rotation is from $\boldsymbol{Z}$ to $\boldsymbol{z}'$, i.e. a rotation vector can be found according to the right hand rule: $\boldsymbol{v}_{rot} = \boldsymbol{Z} \times \boldsymbol{z}'$. The angle of rotation is $\theta_{rot} = \arccos(\boldsymbol{Z} \cdot \boldsymbol{z}')$, where $(\boldsymbol{Z} \cdot \boldsymbol{z}')$ is the dot product between $\boldsymbol{Z}$ and $\boldsymbol{z}'$. The result of implementing Rodrigues' formula is a rotation matrix R, such that $(X, Y, Z)^T = R\,(x_l, y_l, z_l)^T$; the projection onto the plane is obtained by setting $Z = 0$, cf. figure 10b.

The resulting set of coordinates (X, Y) need to be fitted to a circle, again in the least-squares sense, which may be displaced from the origin. If the fitted circle has a center (X_c, Y_c), by taking $(X, Y) \to (X - X_c, Y - Y_c)$, the center of the circle can be made to coincide with the origin of the axes. Then each projected on the plane data point represents the point closest to the circle. Once all these steps are accomplished, determining the angle set $\boldsymbol{\Theta}$ becomes straightforward.

For example, given the stereo images in figure 9, the results of the data extraction are shown in figure 10. Stereo triangulation, in the frame of reference of the left camera yields the position of spikes as displayed in figure 10a. After fitting to a plane and rotation to the laboratory frame of reference (not shown), one can see that the variance in the Z-direction is much less than the crown size in the (X, Y)-plane. This fact confirms the expectation that the tips of the spikes of the crown are nearly coplanar. Next step is to fit the data to a circle, using least square approach, the result of which is given in 10b.

3. *Remarks*

As in any experiments, the collected data are subject to experimental errors and uncertainties, which can be divided into two categories. The first type of errors is due to instrumentation imprecisions. The second type of errors comes from data reduction and analysis. For example, the error in determining the pixel coordinates of corresponding spikes is due to how well the same spike location can be identified in each image. All three factors – spike definition, camera focus, and resolution – contribute to the uncertainty in data reduction.

B. Examples of data analysis

In this section, we demonstrate the analysis of three data sets from the drop splash experiments. The three patterns we have chosen are aimed at illustrating a regular pattern, which has a substantial scatter but is still identifiable[31], an irregular pattern, and a frustrated pattern exemplified in figure 1b: these are the cases of real experimental data which are most interesting from the point of view of the analysis presented here.

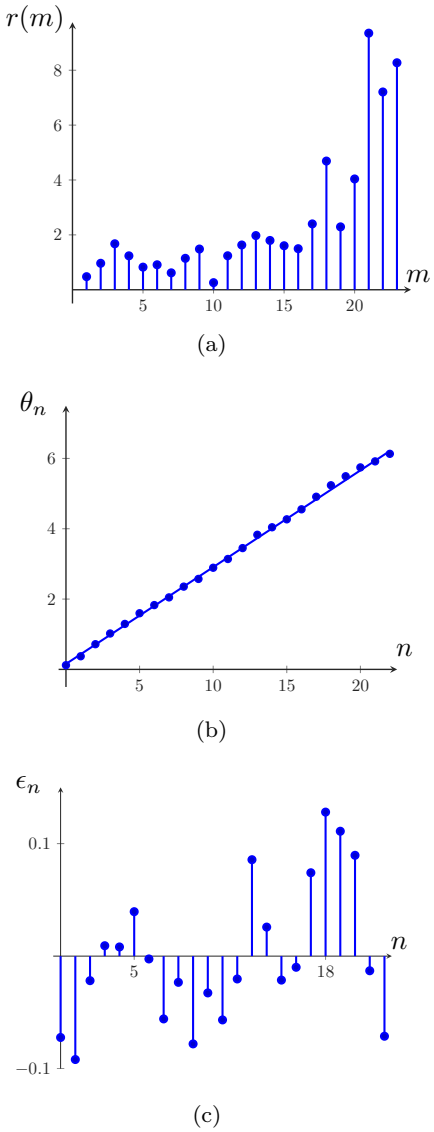

FIG. 11: Example of data analysis for the regular crown with experimental scatter shown in figure 9: (a) moments $r(m)$ of the complex order parameter (6) for the function in figure 10b, (b) extracted angles (dots) and the least square fit (line) according to (7) with $\lambda = 2\pi/k$, $k \in \mathbb{N}$, (c) residuals of the least square fit in figure 11b, cf. definition 3.

C. A regular pattern with substantial scatter

The generalized complex order parameter (6), while suggesting some clustering of data, shows the lack of a clear single dominating order between the dominant values $m = 21, 22, 23$. Therefore the order parameter plot is inconclusive,

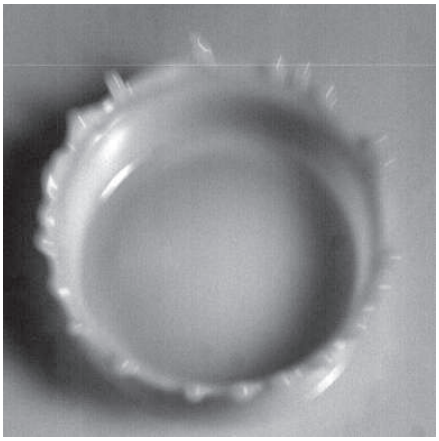

FIG. 12: Right image of the irregular crown.

but still may be interpreted as indicating the possible presence of a single-wavenumber pattern with considerable scatter.

Following the algorithm developed in the proof of theorem 2, we arrive at the graph θ_n in figure 11b, which clearly suggests that the pattern is complete with single-wavenumber $k = 23$ and scatter $\delta \simeq 0.94\,\lambda$. The substantial scatter ratio δ/λ so close to unity (compare to the conditions in theorem 2) indicates that, while it conforms with the definition 3 of a single-wavenumber with scatter[32], the fit is far from ideal according to theorem 2. The fact that the pattern is still identifiable despite $\delta \simeq 0.94\,\lambda$ implies that the condition $\lambda > 2\,\delta$ in theorem 2 is sufficient, but not necessary.

D. An irregular pattern

Now let us consider the apparently irregular crown pattern shown in figure 12. From this figure, we may expect that interpreting the data as a complete single-wavenumber pattern with some scatter is inappropriate. It is notable that the complex order parameter amplitudes in figure 13a do not suggest any dominate wavenumber(s). With the assumption that there are no overlaps and missing points, based on the algorithm developed in the proof of theorem 2, one concludes that the pattern is irregular. The latter fact is also evidenced by the attempted fit of the data to a single-wavenumber pattern in figure 13b exhibiting the scatter (cf. figure 13c) substantially larger than the wavelength!

E. A frustrated pattern

An finally, we would like to 'decipher' the pattern in figure 1b, which will serve as an illustration of both a superposition of several single-wavenumber patterns and overlapping points. Naturally, the DFT and order parameter approaches are not helpful in this case and thus not discussed. The single-wavenumber patterns are identified with the help of the algorithm in the proof of theorem 3 leading to the plot $\theta(n)$ in

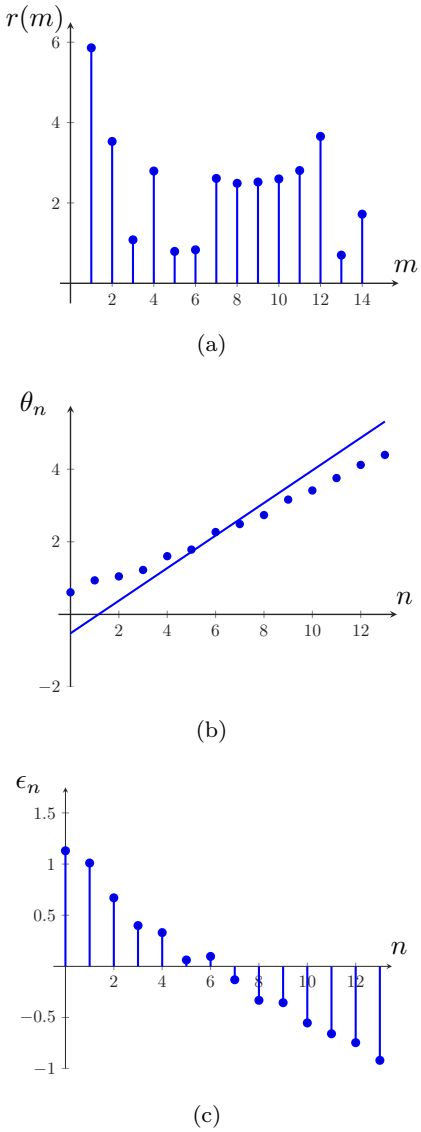

FIG. 13: Example of data analysis in the case of the irregular pattern shown in figure 12: (a) moments of the complex order parameter (6) for the function in figure 12, (b) extracted angles (dots) and the least square fit (line) according to (7) with $\lambda = 2\pi/k$, $k \in \mathbb{N}$, (c) Residuals of the least square fit in figure 13b.

figure 14a; the complete pattern decomposition is shown in figure 14b.

As one can see from the latter figure, there are 5 overlapping points, which is hinted, in particular, by the larger size of the corresponding spikes in figure 1b. While it may appear that given random initial conditions the odds of 5 coinciding spikes are very low, the surface tension effect tends to minimize the surface area. Therefore, if there are two close enough spikes and the time evolution of the crown is sufficiently slow, surface tension will have time to force the spikes to merge similar to a coalescence of liquid drops.

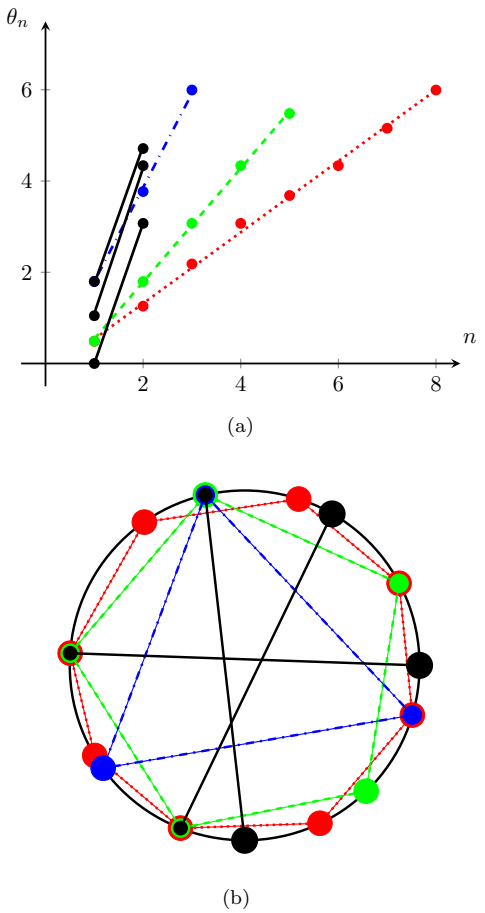

FIG. 14: (Color online) On decomposition of the crown pattern in figure 1b into single-wavenumber patterns: (a) extracted angles (dots) and the least square fit (line) according to (7) with $\lambda = 2\pi/k$, $k \in \mathbb{N}$, the slope of which gives the wavelength of each single-wavenumber pattern: $k = 8$ (dotted), $k = 5$ (dashed), $k = 3$ (dotted-dashed), and three patterns with $k = 2$ (solid). The scatter bound of such a decomposition is $\delta \simeq 0.075$. Note that there are several overlapping points at $\theta = 28°, 103°, 176°, 248.5°, 343.5°$, (b) superposition of single-wavenumber structures giving rise to the crown pattern in figure 1b.

V. CONCLUSIONS

In this Letter we offered a theoretical approach for pattern identification in the wavenumber space. At its basis is the case of ideal patterns without scatter. Effects of scatter and overlaps are then introduced as a generalization of the ideal pattern identification algorithm; conditions for pattern identification are established systematically. This theoretical approach is applicable to a broad range of physical problems with $S(1)$ symmetry on spatial and time domains. The case of incomplete patterns remains a challenge, though a step has been taken towards defining such patterns and understanding of the conditions when they are identifiable. Another potentially interesting extension of the pattern identification theory could be to quasipatterns, i.e. which satisfy $f(x + T) = e^{ax+b} f(x)$ with quasiperiod T and some constants a and b.

To illustrate the theory, a novel experimental method is developed to produce the data suitable for the pattern identification analysis of the crowns resulting from drop splashing. In particular, we used stereo triangulation and data reduction procedure to identify the angular position of each crown spike and applied the theory to a regular pattern with scatter, as well as to irregular and frustrated patterns.

Acknowledgments

This work was partially supported by the National Science Foundation CAREER award under Grant No. 1054267. The authors would like to thank Professors Yuan-Fang Wang and Jeff Moehlis for the helpful discussions, and Hans Mayer for reading over the manuscript.

[1] S. H. Strogatz. From Kuramoto to Crawford: exploring the onset of synchronization in populations of coupled oscillators. *Physica D*, 120:1–20, 2000.
[2] E. Knobloch. Oscillatory convection in binary mixtures. *Phys. Rev. E*, 34:1538–1549, 1986.
[3] V. Ossenkopf, M. Krips, and J. Stutzki. Structure analysis of interstellar clouds. 485:719–727, 2008.
[4] A. Marcu, G. Mocanu, and B. Orza. Standing waves in a solar periodic structures. In V. Mioc, C. Dumitrache, and N. A. Popescu, editors, *Exploring the Solar system and the Universe*, pages 314–317, 2008.
[5] G. Tsiropoula, C. E. Allissanrakis, and D. Dialetis. Periodic and non-peridic phenomena is a sunspot region. *Solar Phys.*, 167:79–94, 1996.
[6] D. Baade. Observed peridic phenomena. In M. A. Smith, H. F. Henrichs, and J. Fabregat, editors, *The Be phenomenon in early-type stars*, pages 1–15. ASP, 2000.
[7] J. Buck. Synchronous rhythmic flashing of fireflies. II. *Quart. Rev. Biol.*, 63:265–289, 1988.
[8] R. Krechetnikov. Stability of liquid sheet edges. *Phys. Fluids*, 22:092101, 2010.
[9] R. Krechetnikov and G. M. Homsy. Crown-forming instability phenomena in the drop splash problem. *J. Colloid Interface Sci.*, 331:555–559, 2009.
[10] R. Krechetnikov. Rayleigh-Taylor and Richtmyer-Meshkov instabilities of flat and curved interfaces. *J. Fluid Mech.*, 625:387–410, 2009.
[11] R. Krechetnikov. A linear stability theory on time-invariant and time-dependent spatial domains with symmetry: the drop splash problem. *Dynamics of PDE*, 8:47–67, 2011.

[12] C. E. Shannon. Communication in the presence of noise. *Proc. Institute of Radio Engineers*, 37:10–21, 1949.
[13] K. V. Mardia. *Directional statistics*. Wiley, Chichester, New York, 2000.
[14] P. Busse and A. Trocińska. Evaluation of orientation experiment data using circular statistics – doubts and pitfalls in assumptions. *Ring*, 21:107–130, 1999.
[15] Y. Kuramoto. *Chemical oscillations, waves, and turbulence*. Springer, Berlin, 1984.
[16] H. Daido. Order function and macroscopic mutual entrainment in uniformly coupled limit-cycle oscillators. *Prog. Theor. Phys.*, 88:1213–1218, 1992.
[17] John R. Taylor. *An introduction to error analysis*. University Science Books, Sausalito, 1997.
[18] W. E. L. Grimson. *From images to surfaces*. MIT press, 1981.
[19] T. A. Clark and J. G. Fryer. The development of camera calibration methods and models. *Photogrammetric Record*, 16:51–66, 1998.
[20] R. Y. Tsai. A versatile camera calibration technique for high-accuracy 3-D machine vision metrology using off-the-shelf TV cameras and lenses. *IEEE J. Robot. Autom.*, RA-3:323–344, 1987.
[21] J. Heikkila and O. Silven. A four-step camera calibration procedure with implicit image correction. In *Proc. of IEEE Computer Vision and Pattern Recognition*, pages 1106–1112, 1997.
[22] Zhengyou Zhang. Flexible camera calibration by viewing a plane from unknown orientations. In *ICCV*, pages 666–673, 1999.
[23] Jean-Yves Bouguet. *Visual methods for three-dimensional modeling*. PhD thesis, Caltech, 1999.
[24] Jean-Yves Bouguet. Camera calibration toolbox for matlab. `http://www.vision.caltech.edu/bouguetj/calib_doc/index.html`, 2008.
[25] A. S. Ogale and Y. Aloimonos. Shape and the stereo correspondence problem. *Int. J. Comp. Vision*, 65:147–162, 2005.
[26] R. W. Brockett. Robotic manipulators and the product of exponentials formula. In P. A. Fuhrmann, editor, *In Mathematical Theory of Networks and Systems. Proceedings of the International Symposium held at the Ben Gurion University of the Negev, Beer Sheva*, pages 120–127. Springer-Verlag, 1984.
[27] It is easy to show that in this case there is a common period for such flashings, i.e. over which the pattern repeats itself.
[28] Since the goal here is to develop practical algorithms, we consider a finite union of single-wavenumber patterns as, from an experimental point of view, an infinite union would be indistinguishable from continuous data. From a theoretical point of view, one can consider an infinite union of single-wavenumber patterns and the resulting pattern would still be formally identifiable with the algorithms presented in the paper.
[29] Otherwise, as easy to conclude, the decomposition of an ideal regular pattern into ideal single-wavenumber patterns is not unique.
[30] For illustration we chose to use images from later (nonlinear) stages of the drop splash evolution, which does not affect the application of the pattern identification method.
[31] Regular patterns with a small amount of scatter are frequently observed (cf. figure 1a), but they are not interesting for the present discussion.
[32] One may reinforce the expectation that the data correspond to a single-wavenumber pattern on physical grounds. First, from the earliest stages in the drop splash recording it is qualitatively clear that the spikes are uniformly spaced [9]. To be able to confidently identify the tips of spikes, it was necessary to wait for the crown to fully develop. Along with the fact that all the spikes to be accounted for are observable, one expects a complete single-wavenumber pattern with scatter.